Advancing the Preparation Strategy of High-Performance Integrated Electrodes for eCO_2RR via Sublimation

Hao Zeng, Xiangbing Zou, Liu Han, Muyao Gao, Yang Liu, Ming Yang, Bing Li*, and, Ming Liu**

Keywords： Metal Phthalocyanine; CO_2RR; Integrated Electrode; Sublimation.

Abstract

The uniform dispersion and loading of phthalocyanine molecular catalysts on conductive carbon substrates are crucial for exposing their active sites. The significant amount of solvent needed to achieve appropriate dispersion of phthalocyanine leads to the risk of re-aggregation during solvent evaporation. Hence, a solventless strategy is sorted by many to bypass the use of solvent. In this study, we showcase the deposition of transition metal phthalocyanines (TMPcs) molecules onto a self-supporting conductive carbon cloth electrode using an environmentally friendly sublimation

technique for efficient electrocatalytic CO_2 reduction. We meticulously investigated the preparation conditions, including heating temperature and TMPcs type, to assess their impact on CO_2 reduction activity. The as-prepared CC-CoPc-450 electrode demonstrated an outstanding comprehensive performance, showcasing a remarkable maximum CO Faradaic efficiency (FE_{CO}) of 97.1% at -0.86V with a current density of 8.3 mA cm^{-2}. Density-functional theory (DFT) calculation demonstrated the role of *d*-orbitals in TM-N_4 and the synergy with π-conjugation electrons in facilitating the efficient electron transfer process in eCO_2RR. This study offers a fresh perspective on the eco-friendly dispersion of TMPcs on conductive substrates and provides insights into the design of π-species macrocyclic electrocatalyst electrodes.

1. Introduction

The conversion of carbon dioxide (CO_2) into value-added fuels and chemicals is one of the effective measures to mitigate greenhouse gas emissions and address energy shortages.[1-8.] Among the various CO_2 conversion technologies, the electrocatalytic CO_2 reduction reaction (eCO_2RR) has attracted considerable attention for its high reaction efficiency and is free from temporal and spatial restrictions.[9-11] However, the applicability is constrained by limited current density and poor product selectivity due to the slow reaction kinetics process, complex reaction pathways, and competitive hydrogen evolution reaction.[12-16] Developing electrocatalysts with high activity and selectivity is an effective measure to promote the further development of eCO_2RR but faces many challenges.

Molecular catalysts hold great promise for eCO_2RR due to their easy accessibility, well-defined molecular structures, and structural tunability at the molecular level.[17-20] However, most molecular-level systems face challenges such as poor catalytic activity and limitations imposed by solubility and the types of solvents used.[21, 22] TMPcs can effectively address these challenges, owing to their robust metal-nitrogen coordination active centers and high structural tailorability. A key requirement is overcoming the intrinsic limitations of TMPcs molecular catalysts, such as poor conductivity due to delocalized electrons within a molecule and aggregation tendencies during the evaporation of the solvent, which impedes the full realization of their catalytic potential. Therefore, integrating molecular catalysts with conductive substrates can pave the way for eCO_2RR, enhancing catalytic activity, conductivity, and structural stability.[4, 23-26] For instance, Liang and colleagues developed a cobalt phthalocyanine/carbon nanotube (CoPc/CNTs) hybrid catalyst through a sonication and magnetic stirring method. The CoPc/CNTs hybrid catalyst containing uniformly dispersed CoPc molecules on the sidewalls of the CNTs delivered a CO Faraday efficiency (FE_{CO}) and partial current density (j_{CO}) as high as 98% and 15.0 mA cm^{-2} at -0.63 V versus RHE, respectively.[27] Lv et al. employed an ultra-thin nitrogen-doped hollow carbon sphere as the anchor support for the CoPc catalyst, which exhibited a high selectivity and current density towards CO.[28] Additionally, Liu et al. synthesized nickel-based phthalocyanine dispersed into carbon nanotubes, achieving an exceptionally high CO selectivity of 99.8%.[25] It is worth mentioning that the aforementioned and most commonly employed methods typically require the use of organic solvents to better disperse the TMPcs molecules. The reliance on organic solvents does not align with the principles of establishing a green economy. Furthermore, the evaporation

of solvents can lead to the re-agglomeration of TMPcs molecules on the substrates, potentially diminishing the number of catalytically active sites.[3, 29, 30] Recently, several studies have employed a sublimation method to disperse TMPcs molecules onto conductive substrates, thereby avoiding the use of solvents and achieving a uniform dispersion of TMPcs molecules.[31, 32] However, the regulation of temperature during sublimation and the state of TMPcs molecules require further exploration. Additionally, the application of sublimation strategies to eCO_2RR is an area that remains to be researched.

To address the research gaps identified in previous works, employing sublimation for the preparation of an Integrated Carbon Dioxide Electroreduction Electrode (ICE) for eCO_2RR was demonstrated. In this work, the effect of sublimation temperature on the state of CoPc molecules and the catalytic performance of ICE were investigated. TG-FTIR and electrochemical tests showed 450˚C was the optimal sublimating temperature for the preparation of high-performance CoPc-ICE preparation. The CoPc molecule is uniformly dispersed on the carbon cloth (CC) substrate. The same approach was used to prepare different types of TMPcs-based ICE to demonstrate the versatility of this method. The Bader charge analysis revealed that the strong covalent interactions between TMPcs and CO_2 are crucial for the activation of CO_2 molecules. Besides, the reduced energy barriers for both *COOH generation and *CO desorption are pivotal contributors to superior catalytic performance. The above results indicate that the preparation of TMPcs integrated electrode by the sublimation strategy is a promising approach and fosters the research of high-performance eCO_2RR integrated electrode catalysts.

2. Experimental

2.1 Carbon cloth treatment

Hydrophobic carbon cloth (W1S1011, Suzhou Sinero Technology) was treated with plasma (150 W for 30 seconds) to enhance its hydrophilicity and denoted as 'CC' prior subsequent treatment process.

100 mg of CoPc (Sigma-Aldrich, purity ≥95%) and a piece of CC (5*5 cm) were placed in a tube furnace. CoPc and CC are placed at the bottom and directly above the porcelain boat heating zone, respectively. The furnace was then ramped to the target temperature at a heating rate of 5˚C/min under an argon atmosphere and maintained for 30 minutes. Upon cooling to room temperature, the phthalocyanine-loaded CC integrated electrode was obtained and denoted as CC-CoPc-T, where T indicates the heating temperature. The residual CoPc powders were collected and denoted as CoPc-450ed. A parallel method was employed to prepare CC-H_2Pc and CC-TMPcs, using H_2Pc, FePc, NiPc, CuPc, and ZnPc as sublimation sources, respectively. To assess the recyclability of the sublimation source, CoPc-450ed was used as the sublimation source. The CoPc deposited on the tube wall was also collected for characterization and named CoPc-Sub.

2.2 Preparation of CoPc@Carbon

20 mg of carbon black was first dispersed in 20 ml of ethanol before 5 mg of CoPc powder was added. The mixture was subjected to ultrasonication for 30 minutes and added to the surface of CC dropwise (100 μL/drop).

3. Results and Discussion

3.1 Formation and Characterization of CoPc ICE

The ICE preparation process via sublimation is depicted in Scheme 1. The solid-state TMPcs molecules underwent gradual sublimation during the heating process in an argon-enriched atmosphere. The sublimated molecules were subsequently captured by the CC and tightly adhered to its surface via π-π interactions, which will facilitate the formation of electron transfer channels during catalysis.

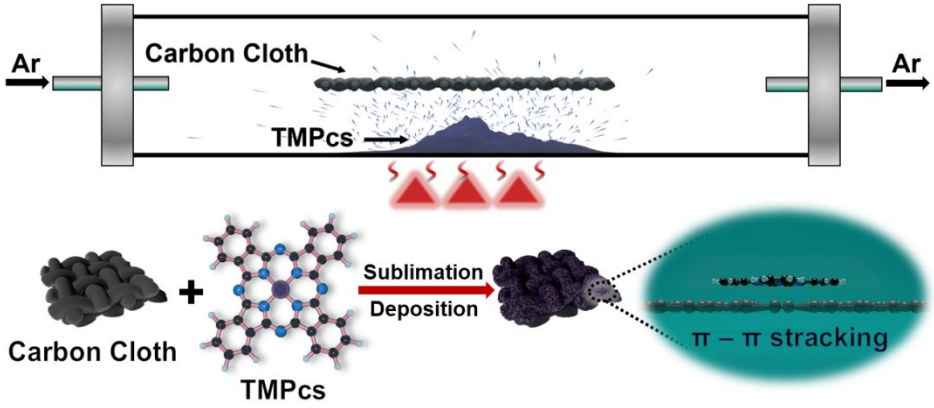

Scheme 1. The schematic illustration of the synthesis process for TMPcs-ICE, and the molecule configurations of a TMPcs stacking under the conductive substrate.

The effect of heating temperature on the molecular structural evolution of CoPc was explored by thermal gravimetric analysis (TGA) (Figure S1) coupled with Fourier Transform Infrared Spectroscopy (FTIR). (Figure 1a) The TGA curve showed a sharp decrease in CoPc mass after 550˚C, indicating the occurrence of thermal degradation of the sample. The TG-FTIR results showed a gradual increase in the intensities of three distinct peaks at 728 cm^{-1} (390˚C), 1122 cm^{-1} (375˚C), and 1350 cm^{-1} (385˚C) from 400˚C onwards, corresponding to CoPc ring vibrations, metal-nitrogen bond stretching, and C-C plane bending in the isoindole structure, respectively.[33]

As the temperature approached 600˚C, the emergence of new characteristic peaks indicated structural changes in the CoPc molecule. Additional details on the identified peaks are presented in Table S1. FT-IR spectra confirmed that the characteristic peaks of CoPc-Sub and CoPc-450ed were consistent with those of the pristine CoPc, indicating that the CoPc molecule can be sublimated without structural damage around 450℃. X-ray diffraction (XRD) spectroscopy further confirmed the unchanged crystal structure of CoPc-450ed after heating treatment (Figure S2). The absence of CoPc diffraction peaks in the CC-CoPc sample suggested that CoPc is either amorphous on the substrate or present in low concentrations, rather than forming distinct particles (Figure S3).[34] X-ray photoelectron spectroscopy (XPS) analysis confirmed the presence of cobalt (Co), carbon (C), nitrogen (N), and oxygen (O) elements in the CC-CoPc-450 catalyst, indicating successful loading of CoPc onto the CC substrate (Figure S4-S6). The presence of Co 2*p* XPS peaks in the CC-CoPc sample further confirmed the successful coupling of CoPc with the CC substrate (Figure 1c). with the peak shift attributed to the strong interaction between the CoPc and the substrate. [35, 36] Scanning electron microscopy (SEM) and energy-dispersive X-ray spectroscopy (EDS) analyses of CC-CoPc-450 samples showed no particle aggregation and uniform distribution of Co and N elements on the CC substrate, respectively (Figure 1d). The collective results from the aforementioned experiments have substantiated the CoPc is evenly and tightly attached to the surface of the CC in the form of molecular dispersion, from multiple perspectives.

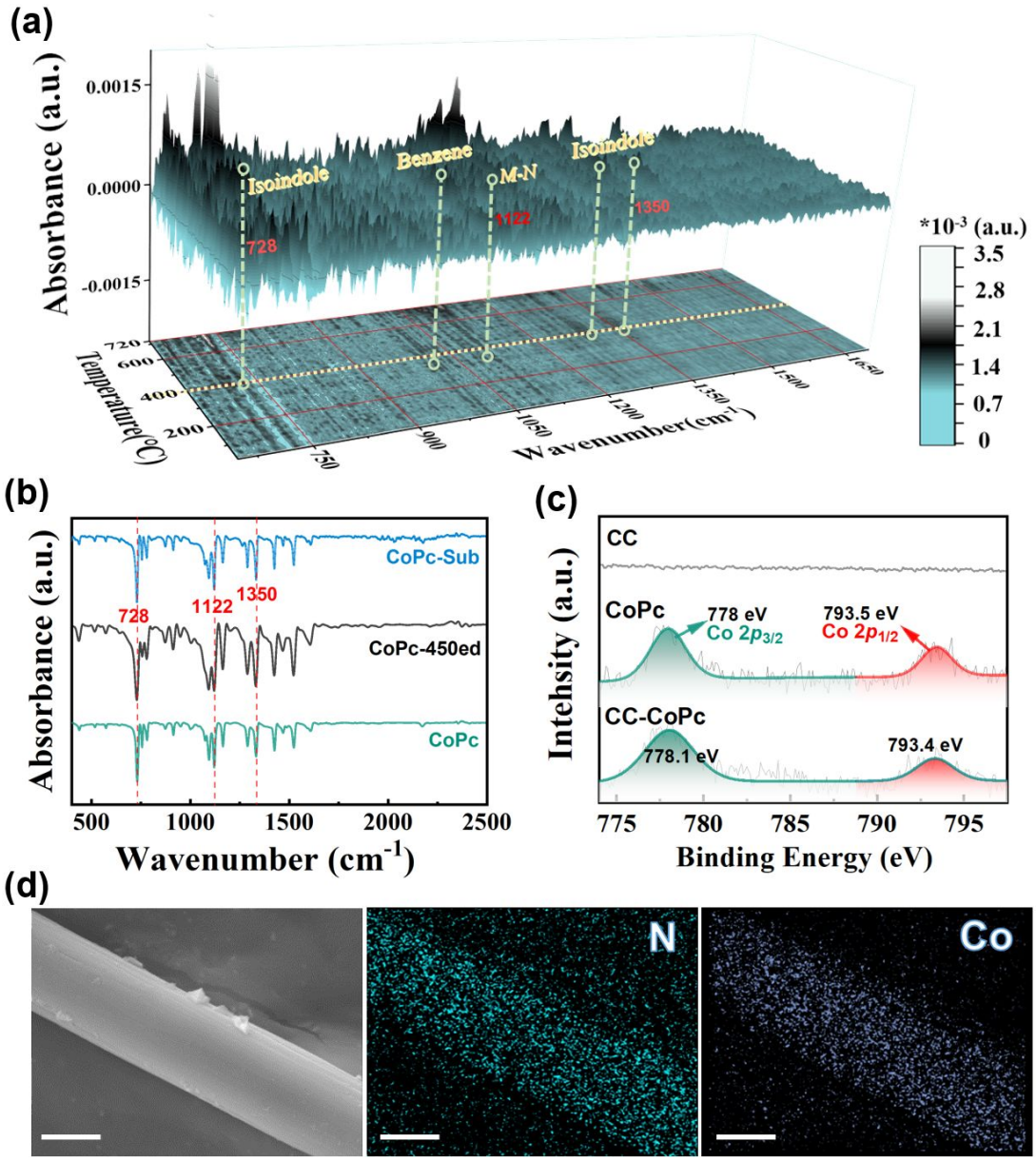

Figure 1. (a) 3D diagrams of TG-FTIR results by CoPc powder; (b) The FT-IR of the sublimation-obtained powder (CoPc-Sub), the remaining volatile sample after sublimation (CoPc-450ed), and the CoPc raw powder (CoPc); (c) The high-resolution XPS of the CC, CoPc powder, and CC-CoPc-450; (d) The SEM and EDS analysis showing the elemental distribution of N and Co in the CC-CoPc-450 sample, with a scale bar of 5 μm.

3.2 Electrochemical eCO_2RR Performance

The electrocatalytic CO_2 reduction performance of the catalysts prepared was assessed in a three-electrode system using Ar/CO_2-saturated 0.5 M $KHCO_3$ as the electrolytes. Ag/AgCl electrodes and commercial graphite rods served as the reference and counter electrodes, respectively. All potentials reported in this study are referenced to the reversible hydrogen electrode (RHE) without *iR* (*i*, current; *R*, resistance) correction. Comparison of the Linear Sweep Voltammetry (LSV) results to Ar-saturated and CO_2-saturated electrolyte, all samples displayed higher current densities and lower onset overpotential in the CO_2 atmosphere, indicative of their eCO_2RR activity (Figure S7). In CO_2-saturated 0.5M $KHCO_3$ solution, CC-H_2Pc (lacking Co center deposition on carbon cloth) and CC showed similar current densities (10 mA/cm^2, -1.2V), whereas CC-CoPc ICE samples exhibited enhanced current densities (18 to 26 mA/cm^2, -1.2V), suggesting the presence of active Co site could effectively promote eCO_2RR (Figure 2a). Notably, the CC-CoPc-450 sample demonstrated the largest current density (26 mA/cm^2, -1.2V) and the lowest onset potential (-0.45V), implying optimal eCO_2RR performance and a lower electrocatalytic reaction energy barrier. The CO_2 reduction performance of ICE was further evaluated by chronoamperometry, and the products were analyzed by gas chromatography (GC). The GC spectra show that the gas products include H_2 and CO, with the total Faradaic efficiency (FE) approaching nearly 100% (Figure S8). CC-CoPc-450 showed excellent CO_2 reduction selectivity, with a Faradaic efficiency for CO (FE_{CO}) exceeding 80% over a board potential range from -0.76 to -0.91 V, peaking at 97.1% at -0.86 V (Figure 2b). At this potential, the FE_{CO} of CC does not show any CO production and CC-H_2Pc was extremely low (12.5%). In contrast, all CC-CoPc samples prepared at different

temperatures demonstrated an FE_{CO} that was significantly higher than 75% (Figure 2c). This more than 6-fold increase in FE_{CO} is strongly associated with the presence of metal-nitrogen coordination sites or alterations in the π-conjugated macrocycle. Moreover, the sublimation temperature significantly influenced the electrocatalytic performance. With FE_{CO} and current density increasing with temperature, peaking at 450˚C (97.1% and 8.3 mA/cm², respectively) for CC-CoPc. At temperatures beyond 450˚C, both parameters declined, possibly due to substrate damage which facilitated the electrolyte penetration and enhanced the hydrogen evolution (Figure S9). More importantly, compared to traditional drop-loading methods, the ICE prepared via the sublimation method has optimized CO selectivity (Figure S10). Additionally, the ICE prepared from the residual CoPc-450ed powder still demonstrated CO selectivity up to 82% at -0.86V, confirming the recyclability of CoPc in this approach (Figure S11).

To investigate the impact of temperature on the eCO_2RR performance of CC-CoPc samples, cyclic voltammetry (CV) tests were conducted at various scan rates within the non-Faradaic region. The results are presented in Figures S12 and 2d. The C_{dl} for CC-CoPc-390, CC-CoPc-410, CC-CoPc-430, CC-CoPc-450 CC-CoPc-470, as well as CC are 0.629, 0.438, 0.524, 0.901, 0.147, and 0.057 μF/cm², respectively. The largest normalized electrochemical-specific surface area corresponds to the highest number of electrochemically active sites, thus exhibiting the optimal eCO_2RR performance among all CC-CoPc samples. Furthermore, CC-CoPc-450 exhibited good stability at -0.86 V, and the FE_{CO} and current density showed no significant decay over a 10800-second long-term potentiostatic test (Figure 2e).

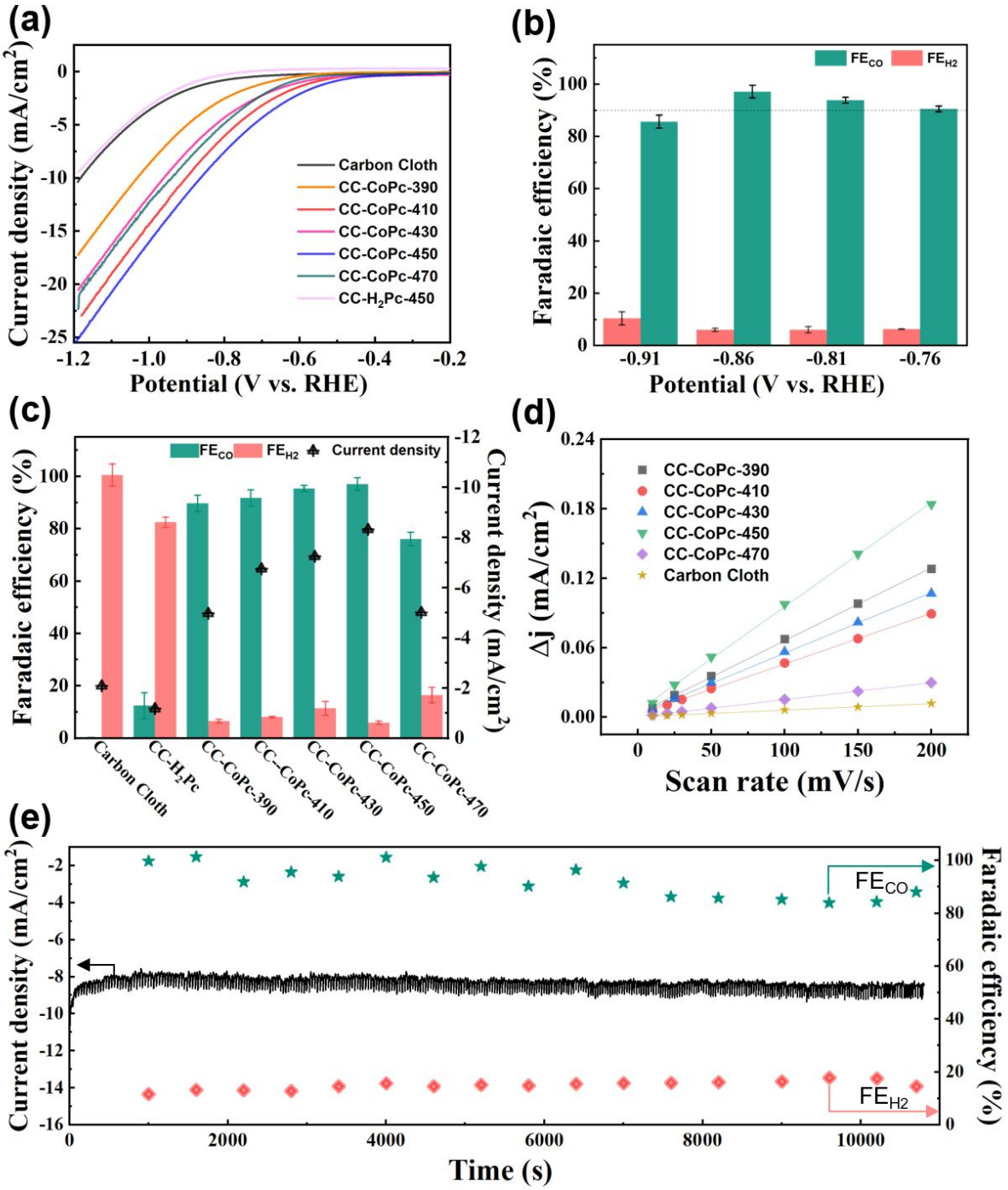

Figure 2. (a) The LSV curve of CoPc-based ICE obtained by different temperature treatments; (b) The FE of CC-CoPc-450 at different potentials; (c) The FE (left axis, columnar) and current density (right axis, star) of different temperatures and sublimation source, the potential settled as -0.86V;

(d) The different ICE of C_{dl} curves; (e) The FE_{CO} (points) and current density curve (line) of CC-CoPc-450, the potential settled as -0.86 V.

3.3 Method universality verification

To ascertain the versatility of the method, ICE samples of various TMPcs (TM = Fe, Ni, Cu, Zn) were prepared using the identical procedure. TGA analysis confirmed that within the temperature range of 300 to 500˚C, all phthalocyanine molecules underwent sublimation and were evenly dispersed on the substrate. SEM and EDS-mapping analyses revealed a uniform distribution of TMPcs molecules across the substrate, with no observable particle aggregation (Figures S14 to S17).

The eCO_2RR performance of the catalysts was further assessed by the H-type cell. The LSV curves revealed that the current densities of all CC-TMPcs-430 and CC-TMPcs-450 samples obtained in the CO_2 atmosphere were markedly higher than in the Ar atmosphere, suggesting robust eCO_2RR activity (Figure S18 and S19). Chronoamperometry was employed to evaluate the CO_2 reduction performance of TMPcs at various potentials (Figures 3a and 3b). Notably, CC-NiPc-430/450 and CC-CoPc-430/450 displayed high CO selectivity across a broad potential range (from -0.66 V to -0.86 V). CC-NiPc-430 achieved an exceptional FE_{CO} of 100% at -0.76 V. In contrast, the FE_{CO} values for CC-FePc-430/450, CC-CuPc-430/450, and CC-ZnPc-430/450 were consistently below 50% across the tested potential range. CC-NiPc-430/450 and CC-CoPc-430/450 exhibited higher CO partial current densities while CC-CoPc-450 reached a peak value of 8.1 mA/cm^2 at -0.86 V. In comparison, the CO partial current densities for CC-FePc-430/450, CC-CuPc-430/450, and CC-ZnPc-430/450 were significantly lower due to their lower CO

selectivity (Figure 3c). These electrocatalysis intrinsic patterns of the TMPcs are aligned with previous studies.[25, 37] The FE_{CO} and current densities of the catalysts prepared in this study surpassed most of the previously reported TMPcs catalysts prepared via the solvent dispersion drop-loading method (Figure 3d and Table S2).

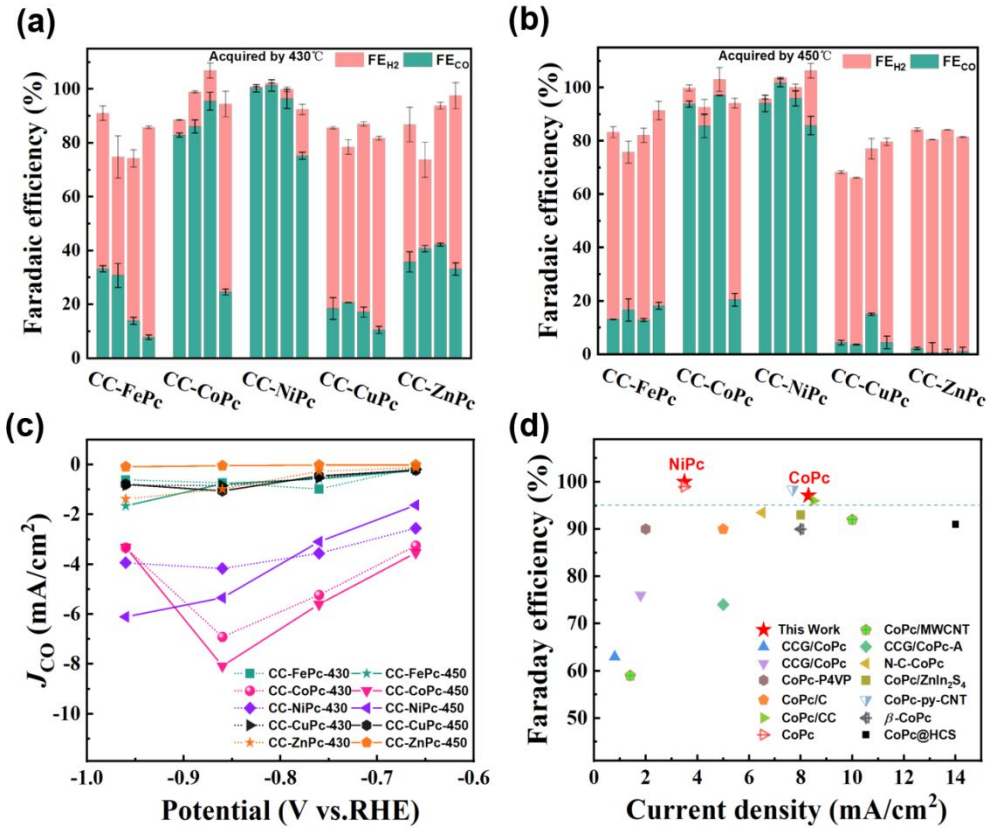

Figure 3. Faraday efficiency of TMPcs catalysts and CC acquired at 430℃ (a) and 450℃ (b), each group of histograms corresponds to the name of the sublimation source below, and the potentials in the group from left to right are -0.66V, -0.76V, -0.86V, and -0.96V, respectively; (c). The partial current density curve of CC-TMPcs-T in different temperatures; (d) Comparison of the best catalytic performance without considering electrolyte and potentials, specific data corresponds to

Table S2, the NiPc From CC-NiPc-430 sample in -0.76V; CoPc comes from CC-CoPc-450 in-0.86V.[11, 38-46]

3.2 Theoretical calculations

Density functional theory (DFT) calculations were conducted to elucidate the mechanism underlying the catalytic reaction. Within this catalytic framework, electron transfer is pivotal for the realization of the catalytic cycle.[47] To delve further into the interactions between the TMPcs molecules and the reaction intermediates, an analysis of charge distributions[48, 49] was undertaken. As depicted in Figures 4a and S20, the primary charge transfer occurs around the M-N_4 active sites and CO_2 molecules and exhibits increased covalency, which facilitates the formation of an effective electron transfer pathway between intermediates and TMPcs. The transferred electrons predominantly originate from the π-conjugation between the metal's d-orbitals and the π-conjugated macrocycles. This redistribution of charge further enhances the M-N_4 redox reactions during the eCO_2RR process. Quantitatively, the charge properties of the molecules follow the trend: CoPc (0.557 e/Bohr^3) > NiPc (0.556 e/Bohr^3) > FePc (0.536 e/Bohr^3) > ZnPc (0.456 e/Bohr^3) > CuPc (0.447 e/Bohr^3). This corresponds to the onset overpotential during the electrochemical test to some extent.

To further elucidate the effects of different TMPcs on catalytic reactions. The DFT calculations of free-energy pathways for CO_2 reduction at the metal sites of TMPcs were performed using the computational hydrogen electrode model.[50-53] The schematic diagrams of intermediate structures are presented in Figure 4b. Among the four elementary reaction steps, the *COOH formation and

*CO desorption reaction energies are significantly dependent on the type of TMPcs. For NiPc, CoPc, CuPc, ZnPc and CC, the *COOH formation was identified as the most endergonic step, determining the overall reaction rate. In contrast, FePc exhibited a higher free-energy barrier (ΔG) for CO desorption, potentially leading to the encapsulation of the catalyst's active sites and affecting the eCO_2RR catalytic process. Considering that the *H intermediate is involved in both the eCO_2RR and HER processes (Figure S21), it influences the selectivity of the final product. The corresponding ΔG values for these intermediates on TMPcs and CC were calculated. Consequently, CuPc, ZnPc, and the CC all exhibited high reaction energy barriers throughout the reaction process (Figure 4c), making electron consumption either for *H generation or *COOH conversion inaccessible. In contrast, CoPc and NiPc, with moderate ΔG, were endowed with optimal catalytic selectivity and electron consumption rates. These results are in perfect agreement with the experimental data, further elucidating the origins of catalytic activity.

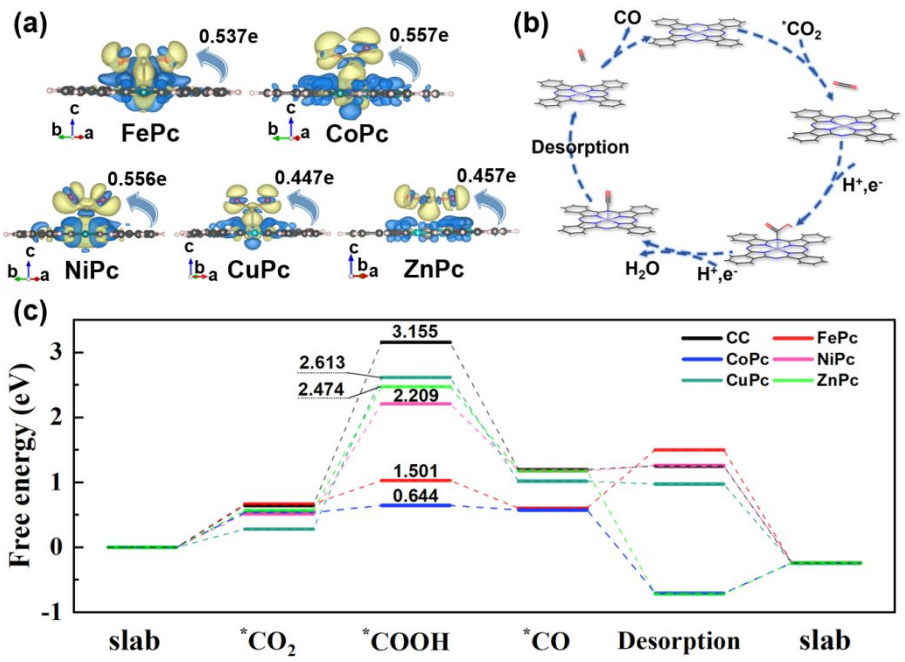

Figure 4. (a). The charge density difference and corresponding charge transfer, yellow parts signify an increase in electrons; blue indicates a decrease; (b). The schematic diagram of the catalytic process of CoPc is shown; (c). The free-energy barrier of eCO_2RR in the catalytic reaction process.

4. Conclusion

In summary, an eco-friendly sublimation strategy was employed to construct an ICE for eCO_2RR. This solventless approach enabled uniform dispersion of TMPcs molecules on π-rich electron surfaces, established a robust pathway for electron transport and thereby enhanced the catalytic efficiency. The CC-CoPc-430/450 and CC-NiPc-430/450 samples exhibited high CO_2 reduction activity and CO selectivity. Particularly noteworthy is the impressive Faradaic efficiency of 97.1% for CO production at -0.86 V and a current density of 8.3 mA cm^{-2} achieved by CC-CoPc-450. The comprehensive catalytic performance of CO_2RR places our system in the top 10%

decile of reported phthalocyanine-based setups. DFT calculations elucidated the *d*-orbitals at the metal center and the π-conjugated macrocycle in TMPcs facilitated effective electron transfer and significantly enhanced catalytic activity. Our work provides a new approach and high efficiency for loading the insoluble catalyst onto conductive substrates which promotes their potential practical applications.

Data Availability

Data will be made available on request.

ASSOCIATED CONTENT

The detailed account of experimental materials and DFT calculations, along with comprehensive information on the testing equipment utilized for TG-FTIR, XPS, XRD, and SEM analyses. Included are the TG curves of transition metal phthalocyanines, LSV results obtained by sublimation strategy sample preparation under different atmospheric conditions, detailed XPS spectra of the samples. The differential charge density maps capturing the electrocatalytic reactions. Additionally, a table outlining the precise peak positions from TG-FTIR analysis and a comparative table of the current-stage metal phthalocyanine-loaded on carbon-based substrates' electrocatalytic performance are provided.

AUTHOR INFORMATION

Corresponding Author

*Ming Yang - *Department of Applied Physics, The Hong Kong Polytechnic University, Hung Hom, Hong Kong SAR, PR China*; ORCID: 0000-0002-0876-1221; E-mail: kevin.m.yang@polyu.edu.hk

* Bing Li - *School of Chemistry and Chemical Engineering, Harbin Institute of Technology, Harbin 150001, PR China*; Email: bing.li2020@hit.edu.cn

*Ming Liu - *School of Chemistry and Chemical Engineering, Harbin Institute of Technology, Harbin 150001, PR China; Engineering Laboratory of Advanced Energy Materials, Ningbo Institute of Materials Technology & Engineering, Chinese Academy of Sciences, Ningbo 315201, PR China*; ORCID: 0000-0002-3243-700X; Email: liuming0117@hit.edu.cn

Authors

Hao Zeng - *School of Chemistry and Chemical Engineering, Harbin Institute of Technology, Harbin 150001, PR China*; ORCID:0000-0001-9148-1716; Email: Haoozeng@sina.com

Xiangbing Zou - *School of Chemistry and Chemical Engineering, Harbin Institute of Technology, Harbin 150001, PR China*; Email: 18846179263@163.com

Liu Han - *School of Chemistry and Chemical Engineering, Harbin Institute of Technology, Harbin 150001, PR China*; Email: 1606276340@qq.com

Muyao Gao - *School of Chemistry and Chemical Engineering, Harbin Institute of Technology, Harbin 150001, PR China*; Email: gaomuyao@foxmail.com

Yang Liu - *MIIT Key Laboratory of Critical Materials Technology for New Energy Conversion and Storage, School of Chemistry and Chemical Engineering, Harbin Institute of Technology, Harbin 150080, PR China*; ORCID: 0000-0001-6475-8943; Email: yang.liu@hit.edu.cn

Funding Sources

This work was supported by the Hong Kong Polytechnic University (project number: P0042711, P0042711and P0048122) and Guangdong Natural Science Foundation (project number: 2024A1515010031).

Notes

The authors declare no competing financial interest.

References

1. Chen, Y.; Li, X.-Y.; Chen, Z.; Ozden, A.; Huang, J. E.; Ou, P.; Dong, J.; Zhang, J.; Tian, C.; Lee, B.-H.; Wang, X.; Liu, S.; Qu, Q.; Wang, S.; Xu, Y.; Miao, R. K.; Zhao, Y.; Liu, Y.; Qiu, C.; Abed, J.; Liu, H.; Shin, H.; Wang, D.; Li, Y.; Sinton, D.;Sargent, E. H., Efficient Multicarbon Formation in Acidic CO_2 Reduction Via Tandem Electrocatalysis. *Nat. Nanotechnol* **2023,** *19* (3), 311-318.
2. Zhou, S.; Zhang, L.; Zhu, L.; Tung, C.;Wu, L., Amphiphilic Cobalt Phthalocyanine Boosts Carbon Dioxide Reduction. *Adv. Mater.* **2023,** *35* (41), 2300923.
3. Wu, Y.; Jiang, Z.; Lu, X.; Liang, Y.;Wang, H., Domino Electroreduction of CO_2 to Methanol on a Molecular Catalyst. *Nature* **2019,** *575* (7784), 639-642.
4. Tan, X.; Yu, C.; Song, X.; Zhao, C.; Cui, S.; Xu, H.; Chang, J.; Guo, W.; Wang, Z.; Xie, Y.;Qiu, J., Toward an Understanding of the Enhanced CO_2 Electroreduction in NaCl Electrolyte over CoPc Molecule-Implanted Graphitic Carbon Nitride Catalyst. *Adv. Energy Mater.* **2021,** *11* (30), 2100075.
5. Han, B.; Ding, X.; Yu, B.; Wu, H.; Zhou, W.; Liu, W.; Wei, C.; Chen, B.; Qi, D.; Wang, H.; Wang, K.; Chen, Y.; Chen, B.;Jiang, J., Two-Dimensional Covalent Organic Frameworks with Cobalt(II)-Phthalocyanine Sites for Efficient Electrocatalytic Carbon Dioxide Reduction. *J. Am. Chem. Soc.* **2021,** *143* (18), 7104-7113.

6. Boutin, E.; Wang, M.; Lin, J. C.; Mesnage, M.; Mendoza, D.; Lassalle-Kaiser, B.; Hahn, C.; Jaramillo, T. F.;Robert, M., Aqueous Electrochemical Reduction of Carbon Dioxide and Carbon Monoxide into Methanol with Cobalt Phthalocyanine. *Angew. Chem. Int. Ed.* **2019,** *58* (45), 16172-16176.
7. Ding, J.; Wei, Z.; Li, F.; Zhang, J.; Zhang, Q.; Zhou, J.; Wang, W.; Liu, Y.; Zhang, Z.; Su, X.; Yang, R.; Liu, W.; Su, C.; Yang, H. B.; Huang, Y.; Zhai, Y.;Liu, B., Atomic High-Spin Cobalt(II) Center for Highly Selective Electrochemical CO Reduction to CH_3OH. *Nat. Commun.* **2023,** *14* (1), 6550.
8. Song, Y.; Guo, P.; Ma, T.; Su, J.; Huang, L.; Guo, W.; Liu, Y.; Li, G.; Xin, Y.; Zhang, Q.; Zhang, S.; Shen, H.; Feng, X.; Yang, D.; Tian, J.; Ravi, S. K.; Tang, B. Z.;Ye, R., Ultrathin, Cationic Covalent Organic Nanosheets for Enhanced CO_2 Electroreduction to Methanol. *Adv. Mater.* **2023,** *36* (17), 2310037.
9. Su, J.; Musgrave, C. B.; Song, Y.; Huang, L.; Liu, Y.; Li, G.; Xin, Y.; Xiong, P.; Li, M. M.-J.; Wu, H.; Zhu, M.; Chen, H. M.; Zhang, J.; Shen, H.; Tang, B. Z.; Robert, M.; Goddard, W. A.;Ye, R., Strain Enhances the Activity of Molecular Electrocatalysts Via Carbon Nanotube Supports. *Nat. Catal.* **2023,** *6* (9), 818-828.
10. Sullivan, I.; Goryachev, A.; Digdaya, I. A.; Li, X.; Atwater, H. A.; Vermaas, D. A.;Xiang, C., Coupling Electrochemical CO_2 Conversion with CO_2 Capture. *Nat. Catal.* **2021,** *4* (11), 952-958.
11. Kramer, W. W.; McCrory, C. C. L., Polymer Coordination Promotes Selective CO_2 Reduction by Cobalt Phthalocyanine. *Chem. Sci.* **2016,** *7* (4), 2506-2515.
12. Zhu, C.; Song, Y.; Dong, X.; Li, G.; Chen, A.; Chen, W.; Wu, G.; Li, S.; Wei, W.;Sun, Y., Ampere-Level CO_2 Reduction to Multicarbon Products Over a Copper Gas Penetration Electrode. *Energy Environ. Sci.* **2022,** *15* (12), 5391-5404.
13. Meng, Z.; Wang, F.; Zhang, Z.;Min, S., Cu Hollow Fiber with Coaxially Grown Bi Nanosheet Arrays as an Integrated Gas-Penetrable Electrode Enables High-Current-Density and Durable Formate Electrosynthesis. *Nanoscale* **2024,** *16* (5), 2295-2302.
14. Dou, T.; Song, D.; Wang, Y.; Zhao, X.; Zhang, F.;Lei, X., Hierarchical Bi/S-Modified Cu/Brass Mesh Used as Structured Highly Performance Catalyst for CO_2 Electroreduction to Formate. *Nano Res.* **2023,** *17* (5), 3644–3652.
15. Song, Y.; Zhang, X.; Xie, K.; Wang, G.;Bao, X., High-Temperature CO_2 Electrolysis in Solid Oxide Electrolysis Cells: Developments, Challenges, and Prospects. *Adv. Mater.* **2019,** *31* (50), 1902033.
16. Zhu, C.; Wu, G.; Chen, A.; Feng, G.; Dong, X.; Li, G.; Li, S.; Song, Y.; Wei, W.;Chen, W., Selective CO_2 Electroreduction to Multicarbon Products Exceeding 2 A cm^{-2} in Strong Acids Via a Hollow-Fiber Cu Penetration Electrode. *Energy Environ. Sci.* **2024,** *17* (2), 510-517.
17. Sa, Y. J.; Jung, H.; Shin, D.; Jeong, H. Y.; Ringe, S.; Kim, H.; Hwang, Y. J.;Joo, S. H., Thermal Transformation of Molecular Ni^{2+}-N_4 Sites for Enhanced CO_2 Electroreduction Activity. *ACS Catal.* **2020,** *10* (19), 10920-10931.

18. Mo, Z.; Zhu, X.; Jiang, Z.; Song, Y.; Liu, D.; Li, H.; Yang, X.; She, Y.; Lei, Y.; Yuan, S.; Li, H.; Song, L.; Yan, Q.;Xu, H., Porous Nitrogen-Rich g-C_3N_4 Nanotubes for Efficient Photocatalytic CO_2 Reduction. *Appl. Catal. B Environ.* **2019,** *256*, 117854.
19. Hu, M.; Wang, N.; Ma, D.;Zhu, Q.-L., Surveying The Electrocatalytic CO_2-to-CO Activity of Heterogenized Metallomacrocycles Via Accurate Clipping at the Molecular Level. *Nano Res.* **2022,** *15* (12), 10070–10077.
20. Ren, S.; Lees, E. W.; Hunt, C.; Jewlal, A.; Kim, Y.; Zhang, Z.; Mowbray, B. A. W.; Fink, A. G.; Melo, L.; Grant, E. R.;Berlinguette, C. P., Catalyst Aggregation Matters for Immobilized Molecular CO_2RR Electrocatalysts. *J. Am. Chem. Soc.* **2023,** *145* (8), 4414-4420.
21. Boutin, E.; Merakeb, L.; Ma, B.; Boudy, B.; Wang, M.; Bonin, J.; Anxolabéhère-Mallart, E.;Robert, M., Molecular Catalysis of CO_2 Reduction: Recent Advances and Perspectives in Electrochemical and Light-Driven Processes with Selected Fe, Ni and Co Aza Macrocyclic and Polypyridine Complexes. *Chem. Soc. Rev.* **2020,** *49* (16), 5772-5809.
22. Zhu, M.; Ye, R.; Jin, K.; Lazouski, N.;Manthiram, K., Elucidating the Reactivity and Mechanism of CO_2 Electroreduction at Highly Dispersed Cobalt Phthalocyanine. *ACS Energy Lett.* **2018,** *3* (6), 1381-1386.
23. Hu, H.; Meng, Y.; Mei, Y.; Hou, P. X.; Liu, C.; Cheng, H. M.; Shao, M.;Li, J. C., Bifunctional Oxygen Electrocatalysts Enriched with Single Fe Atoms and $NiFe_2O_4$ Nanoparticles for Rechargeable Zinc-Air Batteries. *Energy Storage Mater.* **2023,** *54*, 517-523.
24. Zhang, X.; Wang, Y.; Gu, M.; Wang, M.; Zhang, Z.; Pan, W.; Jiang, Z.; Zheng, H.; Lucero, M.; Wang, H.; Sterbinsky, G. E.; Ma, Q.; Wang, Y.-G.; Feng, Z.; Li, J.; Dai, H.;Liang, Y., Molecular Engineering of Dispersed Nickel Phthalocyanines on Carbon Nanotubes for Selective CO_2 Reduction. *Nat. Energy.* **2020,** *5* (9), 684-692.
25. Chen, K.; Cao, M.; Lin, Y.; Fu, J.; Liao, H.; Zhou, Y.; Li, H.; Qiu, X.; Hu, J.; Zheng, X.; Shakouri, M.; Xiao, Q.; Hu, Y.; Li, J.; Liu, J.; Cortés, E.;Liu, M., Ligand Engineering in Nickel Phthalocyanine to Boost the Electrocatalytic Reduction of CO_2. *Adv. Funct. Mater.* **2022,** *32* (10), 2111322.
26. Kornienko, N.; Zhao, Y.; Kley, C. S.; Zhu, C.; Kim, D.; Lin, S.; Chang, C. J.; Yaghi, O. M.;Yang, P., Metal-Organic Frameworks for Electrocatalytic Reduction of Carbon Dioxide. *J. Am. Chem. Soc.* **2015,** *137* (44), 14129-14135.
27. Zhang, X.; Wu, Z.; Zhang, X.; Li, L.; Li, Y.; Xu, H.; Li, X.; Yu, X.; Zhang, Z.; Liang, Y.;Wang, H., Highly Selective and Active CO_2 Reduction Electrocatalysts Based on Cobalt Phthalocyanine/Carbon Nanotube Hybrid Structures. *Nat. Commun.* **2017,** *8* (1), 14675.
28. Gong, S.; Wang, W.; Xiao, X.; Liu, J.; Wu, C.;Lv, X., Elucidating Influence of the Existence Formation of Anchored Cobalt Phthalocyanine on Electrocatalytic CO_2-To-CO Conversion. *Nano Energy* **2021,** *84*, 105904.
29. Liu, Y.; McCrory, C. C. L., Modulating the Mechanism of Electrocatalytic CO_2 Reduction by Cobalt Phthalocyanine Through Polymer Coordination and Encapsulation. *Nat. Commun.* **2019,** *10* (1), 1683.

30. Ren, S.; Joulié, D.; Salvatore, D.; Torbensen, K.; Wang, M.; Robert, M.;Berlinguette, C. P., Molecular Electrocatalysts Can Mediate Fast, Selective CO_2 Reduction in a Flow Cell. *Science* **2019,** *365* (6451), 367-369.
31. Mo, Q.; Meng, Y.; Qin, L.; Shi, C.; Zhang, H.; Yu, X.; Rong, J.; Hou, P.; Liu, C.; Cheng, H.;Li, J., Universal Sublimation Strategy to Stabilize Single-Metal Sites on Flexible Single-Wall Carbon-Nanotube Films with Strain-Enhanced Activities for Zinc-Air Batteries and Water Splitting. *ACS Appl. Mater. Interfaces* **2024,** *16* (13), 16164-16174.
32. Jiang, L.; Gu, M.; Zhao, S.; Wang, H.; Huang, X.; Gao, A.; Zhu, H.; Sun, P.; Liu, X.; Lin, H.;Zhang, X., Regulating the Active Sites of Metal-Phthalocyanine at the Molecular Level for Efficient Water Electrolysis: Double Deciphering of Electron-Withdrawing Groups and Bimetallic. *Small* **2023,** *19* (11), 2207243.
33. Seoudi, R.; El-Bahy, G. S.;El Sayed, Z. A., FTIR, TGA and DC Electrical Conductivity Studies of Phthalocyanine and its Complexes. *J. Mol. Struct.* **2005,** *753* (1), 119-126.
34. Wu, X.; Sun, J. W.; Liu, P. F.; Zhao, J. Y.; Liu, Y.; Guo, L.; Dai, S.; Yang, H. G.;Zhao, H., Molecularly Dispersed Cobalt Phthalocyanine Mediates Selective and Durable CO_2 Reduction in a Membrane Flow Cell. *Adv. Funct. Mater.* **2022,** *32* (11), 2107301.
35. Kong, X.; Liu, G.; Tian, S.; Bu, S.; Gao, Q.; Liu, B.; Lee, C.; Wang, P.;Zhang, W., Coupling Cobalt Phthalocyanine Molecules on 3D Nitrogen-Doped Vertical Graphene Arrays for Highly Efficient and Robust CO_2 Electroreduction. *Small* **2022,** *18* (51), 2204615.
36. Wang, X.; Cai, Z.; Wang, Y.; Feng, Y.; Yan, H.; Wang, D.;Wan, L., In-Situ Scanning Tunneling Microscopy of Cobalt-Phthalocyanine-Catalyzed CO_2 Reduction Reaction. *Angew. Chem. Int. Ed.* **2020,** *59* (37), 16098-16103.
37. Soucy, T. L.; Dean, W. S.; Zhou, J.; Rivera Cruz, K. E.;McCrory, C. C. L., Considering the Influence of Polymer-Catalyst Interactions on the Chemical Microenvironment of Electrocatalysts for the CO_2 Reduction Reaction. *Acc. Chem. Res.* **2022,** *55* (3), 252-261.
38. Han, N.; Wang, Y.; Ma, L.; Wen, J.; Li, J.; Zheng, H.; Nie, K.; Wang, X.; Zhao, F.; Li, Y.; Fan, J.; Zhong, J.; Wu, T.; Miller, D. J.; Lu, J.; Lee, S.-T.;Li, Y., Supported Cobalt Polyphthalocyanine for High-Performance Electrocatalytic CO_2 Reduction. *Chem* **2017,** *3* (4), 652-664.
39. Bhardwaj, A.; Kaur, J.; Wuest, M.;Wuest, F., In-Situ Click Chemistry Generation of Cyclooxygenase-2 Inhibitors. *Nat. Commun.* **2017,** *8* (1), 1.
40. Ma, J.; Zhu, H.;Zheng, Y., Highly Dispersed Cobalt Phthalocyanine on Nitrogen-Doped Carbon Towards Electrocatalytic Reduction of CO_2 to CO. *Ionics* **2021,** *27* (6), 2583-2590.
41. Zhu, M.; Chen, J.; Guo, R.; Xu, J.; Fang, X.;Han, Y., Cobalt Phthalocyanine Coordinated to Pyridine-Functionalized Carbon Nanotubes with Enhanced CO_2 Electroreduction. *Appl. Catal. B Environ.* **2019,** *251*, 112-118.
42. Chen, C.; Sun, X.; Yang, D.; Lu, L.; Wu, H.; Zheng, L.; An, P.; Zhang, J.;Han, B., Enhanced CO_2 Electroreduction Via Interaction of Dangling S Bonds and Co Sites in Cobalt Phthalocyanine/$ZnIn_2S_4$ Hybrids. *Chem. Sci.* **2019,** *10* (6), 1659-1663.

43. Ma, J.; Zhu, H.; Zheng, Y.;Shui, M., An Insight into Anchoring of Cobalt Phthalocyanines onto Carbon: Efficiency of the CO_2 Reduction Reaction. *ACS Appl. Energy Mater.* **2021,** *4* (2), 1442-1448.

44. BaQais, A.; Ait Ahsaine, H., β-Cobalt Phthalocyanine Sono-Immobilized on Carbon Cloth for Efficient Electrochemical Reduction of CO_2-to-CO. *Mater. Lett.* **2022,** *324*, 132614.

45. Xia, Y.; Kashtanov, S.; Yu, P.; Chang, L.; Feng, K.; Zhong, J.; Guo, J.;Sun, X., Identification of Dual-Active Sites in Cobalt Phthalocyanine for Electrochemical Carbon Dioxide Reduction. *Nano Energy* **2020,** *67*, 104163.

46. Wu, X.; Zhao, J. Y.; Sun, J. W.; Li, W. J.; Yuan, H. Y.; Liu, P. F.; Dai, S.;Yang, H. G., Isolation of Highly Reactive Cobalt Phthalocyanine via Electrochemical Activation for Enhanced CO_2 Reduction Reaction. *Small* **2023,** *19* (23), 2207037.

47. Chen, G.; Yuan, Y.; Jiang, H.; Ren, S.; Ding, L.; Ma, L.; Wu, T.; Lu, J.;Wang, H., Electrochemical Reduction of Nitrate to Ammonia Via Direct Eight-Electron Transfer Using a Copper-Molecular Solid Catalyst. *Nat. Energy.* **2020,** *5* (8), 605-613.

48. Zhong, L.; Zhang, L.;Li, S., Understanding the Activity of Carbon-Based Single-Atom Electrocatalysts from Ab Initio Simulations. *ACS Mater. Lett.* **2021,** *3* (1), 110-120.

49. Gu, H.; Zhong, L.; Shi, G.; Li, J.; Yu, K.; Li, J.; Zhang, S.; Zhu, C.; Chen, S.; Yang, C.; Kong, Y.; Chen, C.; Li, S.; Zhang, J.;Zhang, L., Graphdiyne/Graphene Heterostructure: A Universal 2D Scaffold Anchoring Monodispersed Transition-Metal Phthalocyanines for Selective and Durable CO_2 Electroreduction. *J. Am. Chem. Soc.* **2021,** *143* (23), 8679-8688.

50. Cheng, T.; Xiao, H.;Goddard, W. A., III, Reaction Mechanisms for the Electrochemical Reduction of CO_2 to CO and Formate on the Cu(100) Surface at 298 K from Quantum Mechanics Free Energy Calculations with Explicit Water. *J. Am. Chem. Soc.* **2016,** *138* (42), 13802-13805.

51. Zhang, Y.; Wang, T.; Wang, F.; Zheng, H.; Zeng, Z.;Li, H., Identifying Hexagonal 2D Planar Electrocatalysts with Strong OCHO* Binding for Selective CO_2 Reduction. *J. Mater. Chem. A* **2023,** *11* (38), 20528-20538.

52. Kour, G.; Mao, X.;Du, A., Computational Screening of Transition Metal-Phthalocyanines for the Electrochemical Reduction of Carbon Dioxide. *J. Phys. Chem. C* **2020,** *124* (14), 7708-7715.

53. Nørskov, J. K.; Bligaard, T.; Logadottir, A.; Kitchin, J. R.; Chen, J. G.; Pandelov, S.;Stimming, U., Trends in the Exchange Current for Hydrogen Evolution. *J. Electrochem. Soc.* **2005,** *152* (3), J23.